Received January 1996
Revised December 1996

Solidification of a superheated fluid in a porous medium: effects of convection

Xiaoli Zhang and T. Hung Nguyen
Department of Mechanical Engineering, Ecole Polytechnique de Montréal, Montréal, Canada

Keywords *Convection, Porous medium, Superheated*

Abstract *The solidification of a superheated fluid-porous medium contained in a rectangular cavity is studied numerically. The bottom and side walls of the cavity are insulated while the top wall is maintained at a constant temperature below the freezing point of the saturating fluid. The study is focused on the effects of superheat on the development of natural convection and heat transfer during the solidification process. For a fluid initially at a temperature above the freezing point, the results obtained by neglecting convection overpredicts the solidification time by about 12 percent for a Rayleigh number of 800. When convection is taken into account, it is found that the solidification process consists of three distinct regimes: the conduction regime, convection regime, and the solidification of the remaining fluid that can be described by the Neumann solution for the solidification of a fluid at its freezing point. The numerical simulations are based on the Darcy-Boussinesq equations, using the front tracking method in a transformed coordinate system. The entire solidification process is described in terms of the evolutions of the streamlines and isotherm patterns, the maximum and average temperatures of the fluid, the interface position, and the heat transfer rate. The parametric domain covered by these simulations is* $0 \le Ra \le 800$, $0 \le St^l \le 0.67$, $St^s = 0.3$ *and* $XL = 1$ *where Ra is the Rayleigh number,* St^l *the liquid Stefan number,* St^s *the solid Stefan number, and XL the aspect ratio of the cavity.*

Nomenclature

c_p = heat capacity, J/kg°C
d = diameter of the porous matrix sphere, m
g = gravitational acceleration, m/s^2
H = height of the cavity, m
h = dimensionless thickness of the unstable layer
k = conductivity, W/m°C
K = permeability, m^2
L = length of the cavity, m
$\mathbf{n}$ = unit vector normal to the solid-liquid interface
Nu = average temperature gradient at the cooled = surface
Nu^i = average temperature gradient at the interface (on the liquid side)
P = pressure, N/m^2
R = $\alpha_e^s \sigma_e^l / \alpha_e^l \sigma_e^s$, diffusivity ratio
Ra = $\lambda g \Delta T^l K H / (\nu \alpha_e^l)$, Rayleigh number, based on the height of the cavity
Ra^e = $Ra T_{max} h$, effective Rayleigh number, based on the thickness of the unstable layer
S = S^*/H, dimensionless interface position
S_h = St^l/St^s, superheat parameter
St^l = $c_p^l \Delta T^l / \phi \Delta h_f$, Stefan number of the liquid phase
St^s = $c_p^l \Delta T^s / \phi \Delta h_f (k_e^s / k_e^l)$, Stefan number of the solid phase
t = $t^* \alpha_e^l / H^2 \sigma^l$, dimensionless time
t_s = solidification time
T^l = $(T^{l*} - T_f^*)/\Delta T^l$, dimensionless temperature in the liquid
T^s = $(T_f^* - T^{s*})/\Delta T^s$, dimensionless temperature in the solid
T_{ave} = average temperature in the liquid
T_i^* = initial superheating temperature, °C
T_c^* = cooling temperature on the top surface, °C
T_f^* = fusion temperature, °C
$\mathbf{V}$ = velocity in the liquid region, m/s
V_n = $V_n^* H / \alpha_e^l$ interface velocity in the direction = normal to the interface
x,y = Cartesian coordinates
XL = L/H, aspect ratio of the cavity

International Journal of Numerical Methods for Heat & Fluid Flow, Vol. 9 No. 1, 1999, pp. 72-91,

This work was supported by the National Sciences and Engineering Research Council of Canada under grants OGP626 and OGP12621.

Greek symbols

α_e^l = $k_e^l/(\rho c)^l$, thermal diffusivity, m^2/s
α_e^s = $k_e^s/(\rho c)^s$, thermal diffusivity, m^2/s
ξ^1,ξ^2 = transformed coordinates in the liquid region
η^1,η^2 = transformed coordinates in the solid region
Δh_f = latent heat of fusion, *J/kg*
ΔT^l = $T_i^*-T_f^*$ temperature scale in the liquid layer, °C
ΔT^s = $T_f^*-T_c^*$, temperature scale in the solid layer, °C
λ = isobaric coefficient of thermal expansion of fluid, $(°C)^{-1}$
μ = viscosity, Ns/m^2
ν = kinematic viscosity, m^2/s
ρ = density, kg/m^3
ϕ = porosity
φ = φ^*/α_e^l, dimensionless stream function
σ = ratio between the heat capacity of the fluid-saturated medium and that of fluid

Superscript

l = the liquid
m = the porous matrix
s = the solid
* = dimensional variables

Subscript

e = effective property of the saturated porous
= medium
f = quantity at fusion point
max = maximum value
min = minimum value
o = a reference value

Introduction

Recently, the problem of phase change in the presence of natural convection has received a growing interest since modern technologies need more precise and systematic control of this type of problem, which still represents one of the most complicated subjects in heat transfer and convective flow.

The first difficulty in predicting the heat transfer and phase change rate is the proper choice of a length scale, as one has to deal with a moving boundary, i.e. with a system characterized by a time-dependent length scale. This can be best illustrated by the freezing or melting of a phase change material (PCM), initially at its fusion temperature, for which an exact closed-form solution was found (the Neumann solution) in terms of a similarity variable $x/\sqrt{t}$. One can thus look at $\sqrt{t}$ as an appropriate length scale within the spirit of a dimensional analysis. This solution, however, only applies to the case of pure conduction (Prud'homme and Nguyen, 1989; Prud'homme *et al.,* 1989). In fact, while the solidification of a bounded fluid layer without superheat as well as the solidification of a semi-infinite fluid medium with superheat can be solved analytically, the case of a bounded fluid layer at a temperature above its freezing point can only be solved numerically, even if convection is neglected (Boger and Westwater, 1967; Chellaiah and Viskanta, 1988; 1989).

In the presence of natural convection, no analytical solution is possible, and much effort is needed to fully uncover the various scales and regimes, even in the simplest phase change problem, viz. the melting of a rectangular solid block, initially at its fusion temperature and subject to an isothermal heating at one of its vertical sides. Recently, Bejan (1989) and Jany and Bejan (1988) have made a detailed analysis of this problem to identify the basic scales of the phenomenon and to construct a heat transfer correlation for the entire melting process. The results, however, do not apply to the case of a subcooled solid which, as pointed out by the authors, "marks the end of the territory we can cover with the scaling law constructed in this paper". In fact, "it is not a question of merely introducing a new dimensionless group (the solid Stefan number), rather it is the challenge of recognizing the time scales of the heat transfer regimes that keep changing on both sides of the liquid-solid interface. In this effort, easy access to numerical

experiments that account for conduction in the solid is essential" (Jany and Bejan, 1988).

Moreover, the problems of convection, either in a fixed phase or in a PCM, can be divided into two categories: convection in a cavity heated from the side, and convection in a cavity heated from below. The onset and evolution of these two types of convection are quite different: when heated from the side, convection arises as soon as a horizontal temperature gradient is induced, however small it may be. On the other hand, when heated from below, the fluid can remain motionless as long as the vertical temperature gradient is not strong enough for the buoyancy to overcome the viscous force. The time scales of these two cases can thus be expected to differ significantly during a phase change process.

This study considers the solidification process in a rectangular porous cavity cooled from above: the fluid is initially at a temperature above its freezing point, and contained in a porous cavity whose bottom and side walls are insulated while the top wall is maintained at a temperature below the freezing temperature. Attention will be focused on the effect of the superheat on the development of the convection flow, and on the heat transfer mechanisms of the various regimes during the process in order to set the stage for the construction of a unified heat transfer correlation.

Specific applications of this study include freezing of soil in cold weather regions, processing and preservation of foodstuffs, moulding of composite materials, etc.

Governing equations

The physical problem considered here is the solidification of a Newtonian fluid in a rectangular cavity containing a porous medium, as shown in Figure 1. The fluid is initially superheated at a uniform temperature T_i^* which is greater than its fusion temperature T_f^*. As $t \geq 0$, a temperature T_c^*, lower than the fusion temperature T_f^*, is imposed on the top wall of the cavity, while all other

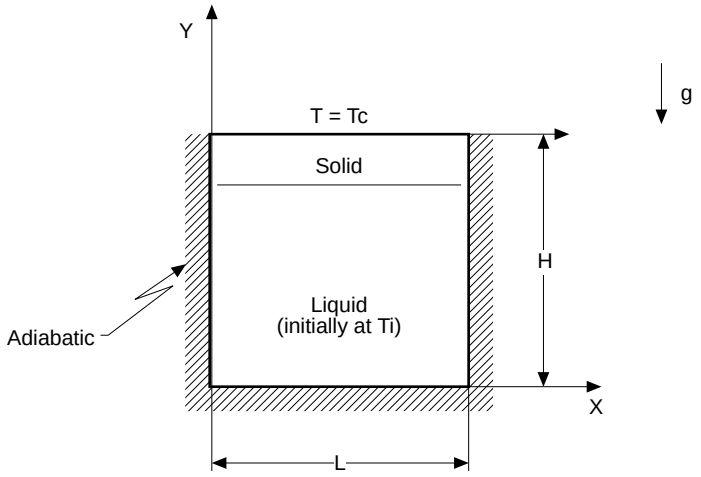

Figure 1.
Geometry of the system

boundaries are maintained adiabatic. As a consequence of this subcooling, a solid layer is formed between the cooled surface and the initially superheated fluid, until the whole cavity is solidified.

In the present model, the following additional assumptions are made for further simplification:

(1) The flow is laminar and two-dimensional.

(2) The liquid is Newtonian and incompressible.

(3) The thermophysical properties are constant except for the density in the buoyancy term (Boussinesq approximation).

(4) The density change due to solidification is negligible (solid density is equal to liquid density).

(5) The Reynolds number based on the pore size is small enough for the Darcy model to be valid, i.e. the effects of inertial force (Forchheimer term) and vorticity diffusion near solid boundaries (Brinkman term) can be neglected.

Under these assumptions, the problem considered in this study can be described by

the continuity equation

$$\nabla \cdot \mathbf{V} = 0 \tag{1}$$

the Darcy equation

$$\mathbf{V} = \frac{K}{\mu}(-\nabla P + \rho \mathbf{g}) \tag{2}$$

the energy equation in the liquid region

$$\sigma_e^l \frac{\partial T^l}{\partial t} + \nabla \cdot \left(\mathbf{V} T^l - \alpha_e^l \nabla T^l\right) = 0 \tag{3}$$

the energy equation in the solid region

$$\sigma_e^s \frac{\partial T^s}{\partial t} - \alpha_e^s \nabla^2 T^s = 0 \tag{4}$$

and the energy balance equation at the interface

$$\rho \phi \Delta h_f V_n = -k_e^l \nabla T^l \cdot \mathbf{n} + k_e^s \nabla T^s \cdot \mathbf{n} \tag{5}$$

where V_n is the interface velocity in the direction **n** normal to the interface.

The buoyancy term in the momentum equation can be determined by the state equation

$$\rho = \rho_f(1 - \lambda(T^l - T_f)) \tag{6}$$

Note that, for the sake of clarity, all dimensional quantities in equations (1)-(6) have been written without superscript*.

By introducing the stream function φ such that $\mathbf{V} = (\varphi_y, -\varphi_x)$, to satisfy the continuity equation, equations (1)–(6) can be reduced to the dimensionless system

$$\nabla^2\varphi + Ra\frac{\partial T}{\partial x} = 0 \tag{7}$$

$$\frac{\partial T^l}{\partial t} + \nabla \cdot (VT^l) = \nabla^2 T^l \tag{8}$$

$$\frac{\partial T^s}{\partial t} - R\nabla^2 T^s = 0 \tag{9}$$

$$V_n = -St^l \nabla_n T^l + St^s \nabla_n T^s \quad \text{(at the interface)}, \tag{10}$$

where

$$Ra = \lambda g K \Delta T^l H/\nu\alpha_e^l$$
$$St^l = c_p^l \Delta T^l/(\Delta h_f \phi)$$
$$St^s = c_p^l \Delta T^s/(\Delta h_f \phi)k_e^s/k_e^l$$
$$R = \alpha_e^s \sigma_e^l/(\alpha_e^l \sigma_e^s)$$

and the dimensional scales

$$\Delta T^l = T_i^* - T_f^*$$
$$\Delta T^s = T_f^* - T_c^*$$
$$\Delta t = H^2 \sigma_e^l/\alpha_e^l$$
$$\Delta x = H$$
$$\Delta y = H$$

are used.

The boundary conditions associated with the non-dimensional equations are:

T = –1, on the top wall

$\frac{\partial T}{\partial n}$ = 0, on the bottom and side walls

φ = 0, on the interface and on the cavity walls

T = 0, on the interface

Note that the condition $\varphi = 0$ on the interface implies normal velocity along the interface is zero, as it has been assumed that density change due to solidification is negligible.

The initial condition is

$$T|_{t=0} = 1$$

In applying the foregoing equations, all quantities are to be taken as their averages over a representative elementary volume. In particular, the mean (effective) thermal capacitance of the liquid-saturated porous region is given by

$$(\rho c)_e^l = \phi(\rho c)^l + (1-\phi)(\rho c)^m$$

while the effective thermal capacitance of the frozen region is

$$(\rho c)_e^s = \phi(\rho c)^s + (1-\phi)(\rho c)^m$$

The effective conductivities can be defined in a similar way.

Note that the coefficients σ in equations (3-4) are the ratios between the effective thermal capacitance and the fluid capacitance, while the αs are the ratios between the effective conductivity and the fluid heat capacitance, in the liquid and solid regions respectively.

The coefficient K that appears in the Darcy equation, defined as the permeability of the pore matrix, essentially depends on the microstructure of the medium. For a packed bed of spheres, K can be expressed in terms of the porosity ϕ and the sphere diameter d as

$$K = \frac{d^2\phi^3}{150(1-\phi)^2}$$

(For example, with d = 3mm and $\phi = 0.4$ $K \approx 10^{-8} m^2$).

Furthermore, due to their similar form, the two dimensionless parameters St^l and St^s have been called the liquid and solid Stefan numbers respectively. Alternatively, one could use a solid Stefan number St^s, and a superheat parameter $S_h = St^l/St^s$. In this problem, the solid Stefan number can be associated with the driving force for solidification , while the liquid Stefan number, or alternatively the superheat parameter, indicates the "resistance" to the solidification process. The competition between these two forces, in controlling the solidification process, is closely related to the evolution of the temperature fields in both the solid and liquid regions, as expressed in the energy balance equation at the interface. Note that the strength of the driving force is controlled by conduction in the solid region while the strength of the resistance force is controlled by both conduction and convection in the liquid region. One should remark in passing that although the liquid Stefan number (or the superheat parameter) and the Rayleigh number are both directly proportional to the temperature difference in the liquid region, it is the Rayleigh number, and not the liquid Stefan number, that indicates the strength of convection. In fact, if no convection can develop (such as in a zero-gravity

environment, or in the case of solidification from below), the liquid Stefan number then indicates the strength of conduction in the superheated liquid region.

Solution method

Owing to the existence of the moving interface S, the solid and liquid domains are irregular and time-dependent. To overcome this difficulty, a curvilinear system of coordinates is used to transform the physical domain into a rectangular region for the computations. The transformations

$$x = \xi^1, \qquad y = S\xi^2$$

and

$$x = \eta^1, \qquad y = (1 - S)\eta^2 + S$$

map the irregular domains into two rectangles,

$$0 \leq \xi^1 \leq 1, \qquad 0 \leq \xi^2 \leq 1$$

and

$$0 \leq \eta^1 \leq 1, \qquad 0 \leq \eta^2 \leq 1$$

for the liquid and the solid regions respectively.

The numerical computation is initiated with a layer of solid of a constant thickness corresponding to an initial interface position $S_0 = 0.95$. The solidification process is simulated until the average interface position reaches the value $S = 0.05$. This choice of S_0 was adopted after tests had been made to ensure that a thinner initial solid layer ($S_0 = 0.98$) did not change the subsequent evolution of the interface in any significant way.

A finite-difference method based on a control volume formulation was used to obtain the numerical solutions. The discretized equations were derived by using a power-law interpolation scheme for the spatial discretization and a standard forward difference approximation for the time derivative. Computational grids of 31×21 and 31×11 are used, respectively, for the liquid and solid domain, with a dimensionless time step of about 10^{-3}. A finer grid size and/or time step only change the results by less than 1 percent for some typical cases considered in this study. Details of the numerical method and the validation of the computer code can be found in Zhang *et al.* (1991). It is worth noting in particular that the updating of the solid/liquid interface was achieved in the following way: at each time step, the interface position S was determined from the energy balance at the interface. The stream function φ, temperature T^l and T^s were then simultaneously solved using ADI technique. The convergence criterion used was that

$$\frac{max \mid \Phi_{ij}^{k+1} - \Phi_{ij}^{k} \mid}{max \mid \Phi_{ij}^{k} \mid} < \varepsilon$$

where Φ is T, S or φ, superscript k is the kth iterative step and ε (10^{-4}) is the typical tolerance. The position of the interface S was then recalculated using the new values of φ and T, this procedure being repeated until converged solutions were obtained. Usually, three to ten iterations were needed at each time step.

Results and discussion

As described in the previous section, the problem of solidification considered here is governed by five dimensionless parameters, namely the Rayleigh number Ra, the Stefan numbers St^l and St^s, the aspect ratio XL and the diffusivity ratio R. The present study is focused on the Rayleigh number and the liquid Stefan number in order to describe the effects of convection on the solidification of an initially superheated fluid. For a given fluid-saturated medium, the Rayleigh number and the fluid Stefan number are parameters that can be changed simultaneously as the initial superheat is changed, since they are both proportional to $\Delta t^l = T_i^* - T_f^*$. The two pairs of parameters (Ra_0, St_0^l) and (Ra_1, St_1^l) are related by

$$Ra_1/Ra_o = St_1^l/St_o^l \tag{11}$$

Hereafter, the various values of Ra and St^l will be expressed in terms of a reference set of values $Ra_0 = 200$ and $St_0^l = 0.1674$. Other parameters are chosen to be $St^s = 0.3068$, $R = 7.366$, $XL = 1$. These parameters have been chosen for water around its fusion point, but should be regarded as representative of a typical range of values under consideration; they do not restrict the validity of the results to any specific fluid. (In fact, as far as water is concerned, the peculiar behavior of density inversion is not considered here. A detailed study on this latter phenomenon was presented in Zhang *et al.* (1991) and Zhang and Nguyen (1990).)

For the case of an initially superheated liquid, it should be noted that as soon as the solidification begins, a very thin thermal boundary layer is formed beneath the solid-liquid interface. This layer is potentially unstable against the Bénard convection as the fluid adjacent to the interface is cooler, therefore heavier, than the fluid underneath. The parameter which controls this type of instability is the ratio between the buoyancy and viscous forces within the layer, namely the effective Rayleigh number

$$Ra^e = RaT_{max}h \tag{12}$$

where T_{max} is the maximum temperature difference within the unstable fluid layer, and h is defined as the dimensionless thickness of the fluid layer comprised between the interface and the isotherm $T^l = 1 - 10^{-4}$ if $T_{max} > 1 - 10^{-4}$; otherwise it is the average thickness of the whole liquid layer.

From this definition it appears that both T_{max} and h, and therefore Ra^e, are functions of time. One should expect that convection will exist only while the effective Rayleigh number is high enough (i.e. above a certain critical value for Bénard convection to be maintained).

In order to evaluate the effect of convection on the solidification of a superheated fluid, let us first consider the results obtained by assuming that pure conduction is the sole mechanism of heat transfer during the whole process.

Solidification by pure conduction

Solutions by pure conduction were obtained from equations (7)-(10) by setting $Ra = 0$.

The evolutions of the maximum temperature T_{max}, the average temperature of the fluid T_{ave}, the average interface position S, and the heat transfer rate at the top of the cavity, are shown in Figures 2-4 for the solidification process ($0.05 \leq S \leq 0.95$). The heat transfer rate is represented by the Nusselt number Nu, which is here defined as the average dimensionless temperature gradient. The average temperature T_{ave} is the arithmetic mean value of the calculated temperature in the liquid region.

Figure 2 corresponds to the particular case of a fluid initially at its fusion temperature ($St' = 0$) for which a closed-form solution exists (Prud'homme *et al.*, 1989). Figures 3-4 correspond to $St' = St'_0$ and $3St'_0$ respectively. Although these figures are rather small to be self-explained, they clearly illustrate the following discussion.

First, for the case presented in Figure 2, the numerical results obtained for the evolutions of the interface position and the Nusselt number agree perfectly with the Neumann solution for the solidification of a fluid initially at its fusion temperature, i.e. the solidified layer grows as $\sqrt{t}$ while the Nusselt number decreases as $1/\sqrt{t}$. Note that the numerical simulation was stopped at $t \approx 1.5$ when $S = 0.05$. It can be then deduced that the time necessary to solidify the

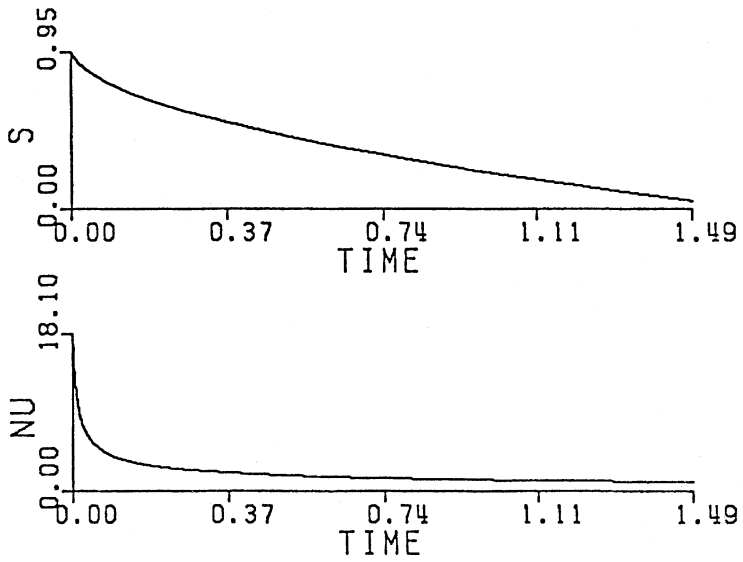

Figure 2.
Evolution of the interface position and heat transfer rate at the cooling surface for $St' = 0$

whole cavity will be $1.2/(1 - 0.05)^2 = 1.65$, and the time for half of the cavity to solidify is 0.41.

When the fluid is initially at a temperature above its fusion point, for example when $St' = St'_0$, it was found that T_{max} remains almost unchanged ($T_{max} \approx 1$) during a short time $t \approx 0.7$ as can be seen from Figure 3. The time for the effect of the subcooling to reach the lower boundary is thus about 10 percent of the time to completely evacuate the superheat, and about 4 percent of the time to solidify the whole cavity. As a consequence, by shifting the time by $t \approx 0.07$, the curves of T_{max} and T_{ave} practically coincide for the rest of the cooling process. The same phenomenon occurs at a higher initial temperature, as shown in Figure 4, for $St' = 3St'_0$. Furthermore, it appears that Figures 2, 3 and 4

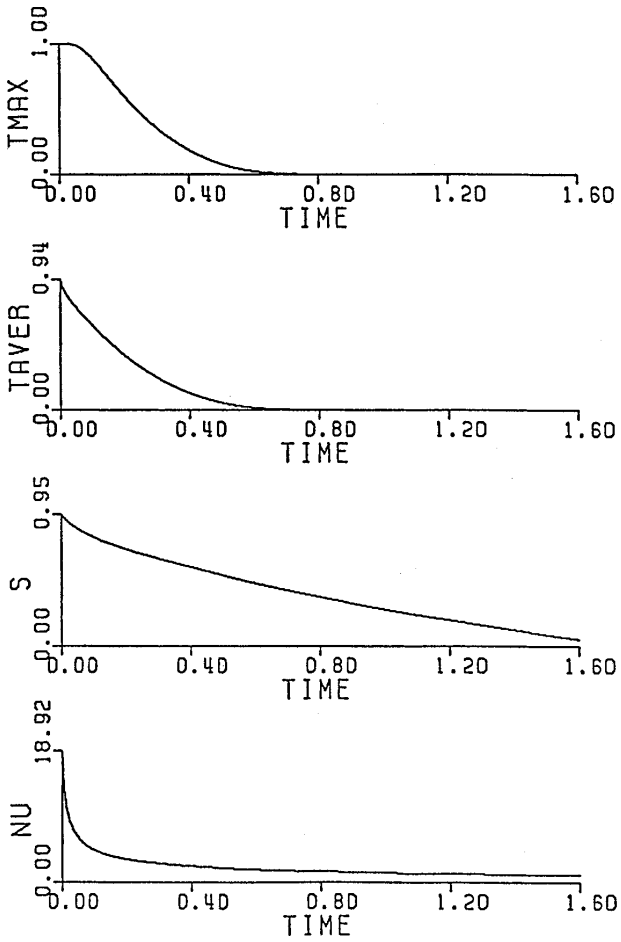

Figure 3.
Evolution of T_{max}, T_{ave}, S and Nu for $St' = St'_0$

corresponding to various liquid Stefan numbers are quite similar. In fact, they coincide when drawn on a time scale $\tau = t/t_s$, except for the average interface curve which slightly changes as St^l is varied from 0 to $3St_0^l$. In other words, if we use a renormalized time $\tau = t/t_s$, we shall obtain a "universal" curve for each of the variables T_{max}, T_{ave}, S and Nu, while Figure 5 provides a correlation between the solidification time t_s and the liquid Stefan number St^l.

Solidification in the presence of convection

Figures 6 and 7 present the evolution of the quantities of interest, viz Ra^e, T_{max}, T_{ave}, φ_{max}, S and Nu for Rayleigh numbers corresponding to the liquid Stefan numbers considered above (note the relationship between Ra and St^l, equation (11)).

Figure 6, for $St^l = St_0^l$, $Ra = Ra_0$ shows that the maximum stream function is attained at $t \approx 0.13$ while the effective Rayleigh number reaches its peak value

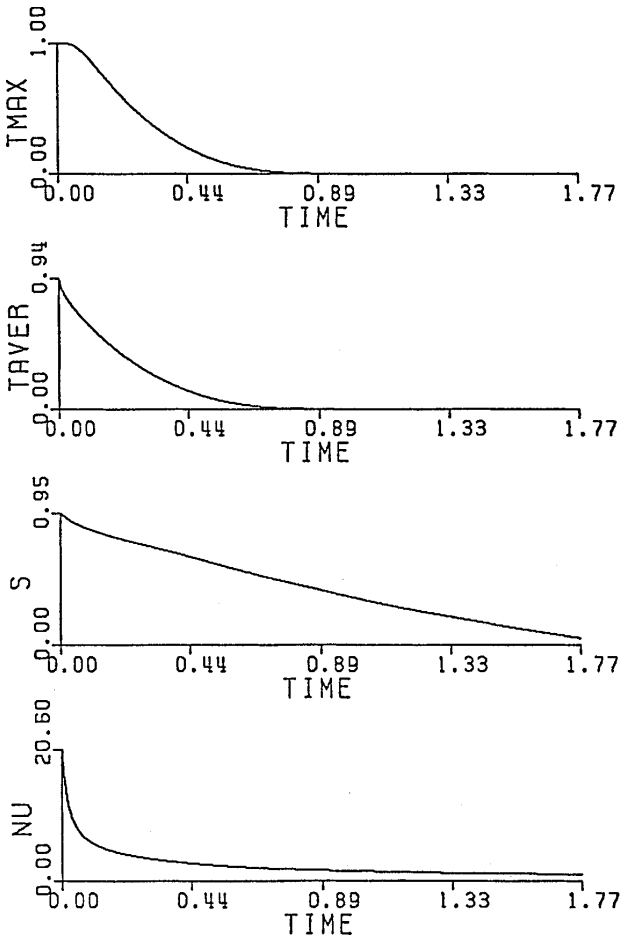

Figure 4.
Evolution of T_{max}, T_{ave}, S and Nu for $St^l = 3St_0^l$

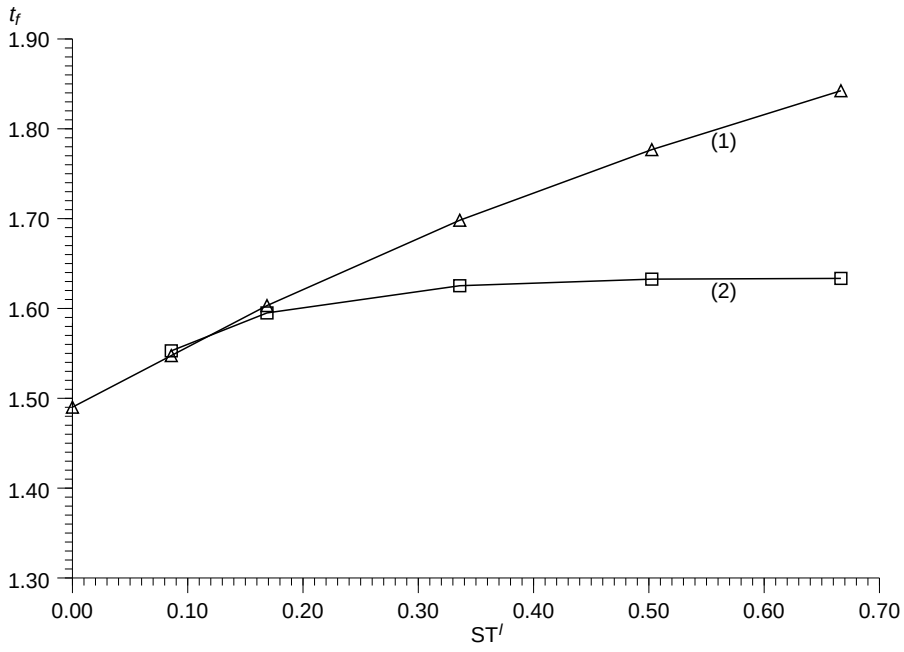

Figure 5. Solidification time vs. liquid Stefan number (a) by conduction only; (2) by convection

($Ra^e \approx 178$) at $t \approx 0.025$. This time lag may be due to the very small growth rate of the disturbances during the initial development of Bénard convection. If it is so, it would be difficult to "match" the onset time of convection as predicted by the stability theory with the "onset time" as observed either in experiments or in numerical simulations. Once convection sets in, the maximum as well as the average temperatures decrease more rapidly than in the previous case while the solidification is slightly slowed down. One notes that the convection activity as indicated by the maximum value of the stream function (φ_{max}) is strongest at $t \approx 0.14$ before decreasing to zero at $t \approx 0.4$. As can be expected, the convective flow enhances the heat transfer rate on the liquid side corresponding to a bell shape of the Nusselt number Nu^i at $t \approx 0.14$ (but not seen on the curve of Nu).

For $St^l = 3St_0^l$, $Ra = 3Ra_0$, Figure 7 shows that convection becomes quite strong ($\varphi_{max} \approx 12.4$) and its onset coincides with the maximum effective Rayleigh number ($Ra^l \approx 559$) at $t \approx 0.015$. The flow becomes, thereafter, negligibly weak at $t \approx 0.4$. The effect of convection is now reflected in both Nusselt numbers, on the liquid side and at the top of the cavity: the onset of convection induces a sharp jump in the curves of Nu versus time. As a consequence of this enhanced heat transfer, the inverse phenomenon of melting occurs at the onset of convection, as can be clearly seen in Figure 8 where the interface position is shown at different times. By noting that the interface movement is governed by the equation $V_n = St^s\frac{\partial T^s}{\partial y} - St^l\frac{\partial T^l}{\partial y}$, the interface velocity V_n can be positive, i.e. melting can occur, if the superheat is high enough for the

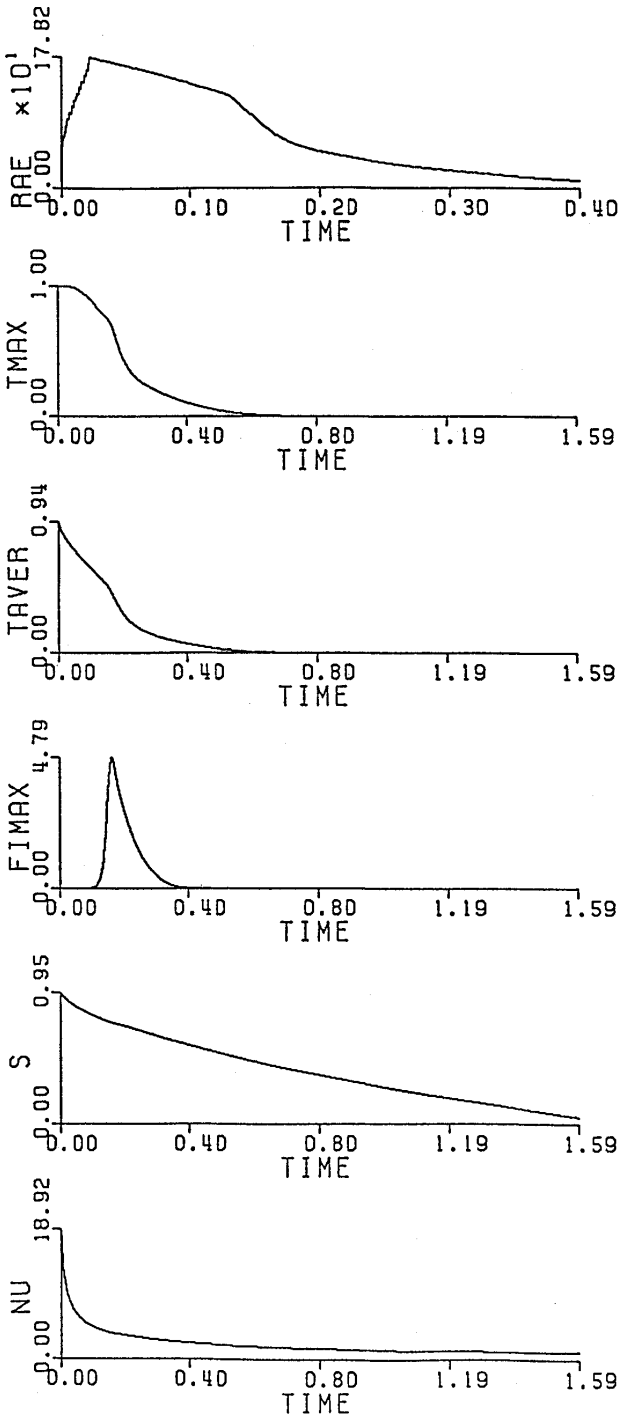

Figure 6.
Evolution of Ra^e, T_{max}, T_{ave}, S and Nu for $St' = St'_0$, $Ra = Ra_0$

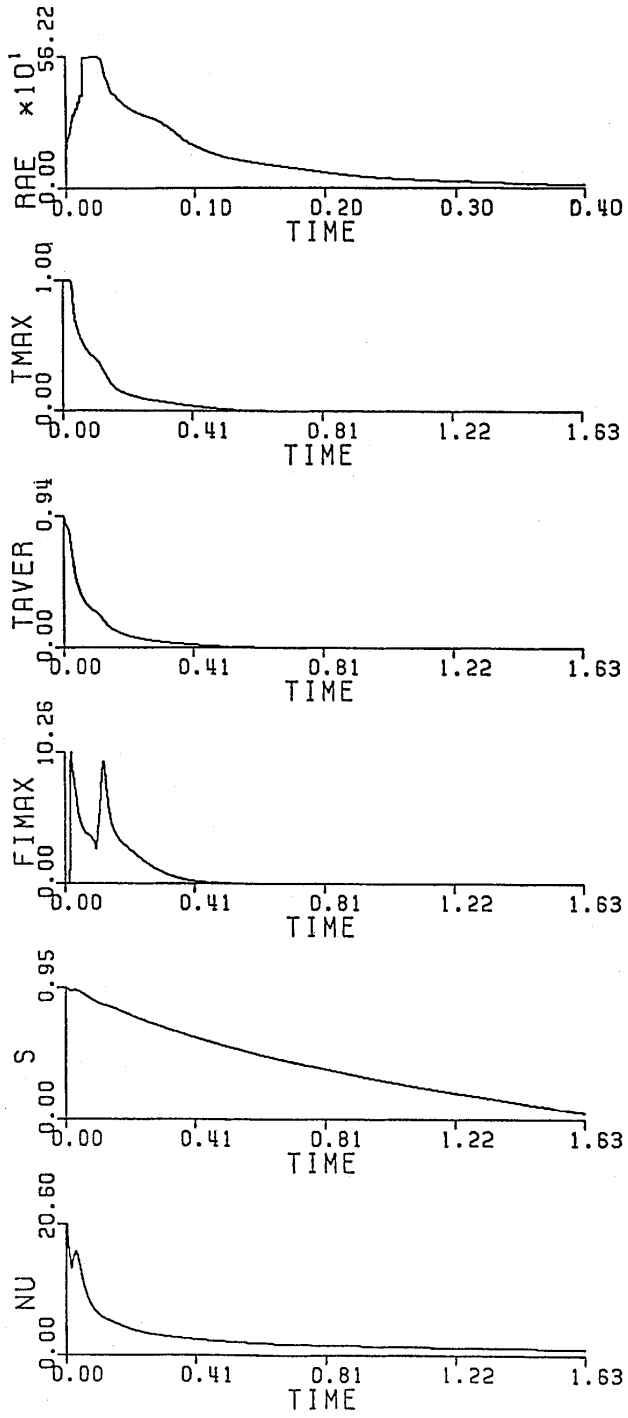

Figure 7.
Evolution of Ra^e, T_{max}, T_{ave}, S and Nu for $St^l = 3St_0^l$, $Ra = 3Ra_0$

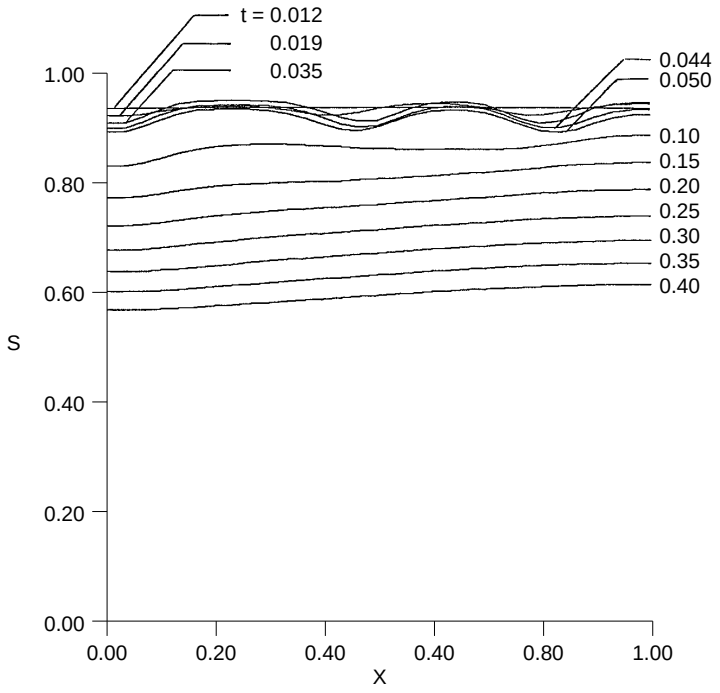

Figure 8.
Interface positions at various times for $St^l = 3St_0^l$, $Ra = 3Ra_0$

heat transfer rate on the liquid side, $-St^l\frac{\partial T^l}{\partial y}$, to become greater than that on the solid side, $-St^s\frac{\partial T^s}{\partial y}$. In fact, as convection arises, the hot fluid impinging on the interface can sufficiently increase the heat transfer to induce a local melting in that area. This melting cannot continue for long as the solid layer gets thinner and more heat is transferred by conduction through the top of the cavity to balance the heat input from the superheated fluid. This phenomenon has been observed in the experiments of Boger and Westwater (1967). Also, in the simulation of melting from below, it was found that refreezing can occur during the transition period of the convection form (Zhang *et al.*, 1991). These results clearly show that the effect of convection is to enhance the cooling of the superheated fluid, and to slow down the solidification process during that time.

The development of the convection flow for $St^l = St_0^l$ and $St^l = 3St_0^l$ respectively is described by the streamlines and isotherms shown in Figures 9 and 10, where the increments between isotherms are $T_{max}/10$ and between streamlines are $(\varphi_{max} - \varphi_{min})/10$. One can remark that at the onset of convection, the flow pattern consists of rather regular cells and the isotherms are nearly horizontal, as can be expected from the Bénard type convection. As convection further develops, the isotherms become more distorted, and the convection cells become more unequal to vanish one by one, until there remains only a residual unicellular flow of negligible strength. As the superheat is increased, the strength and the number of convection cells also increases. One can also note

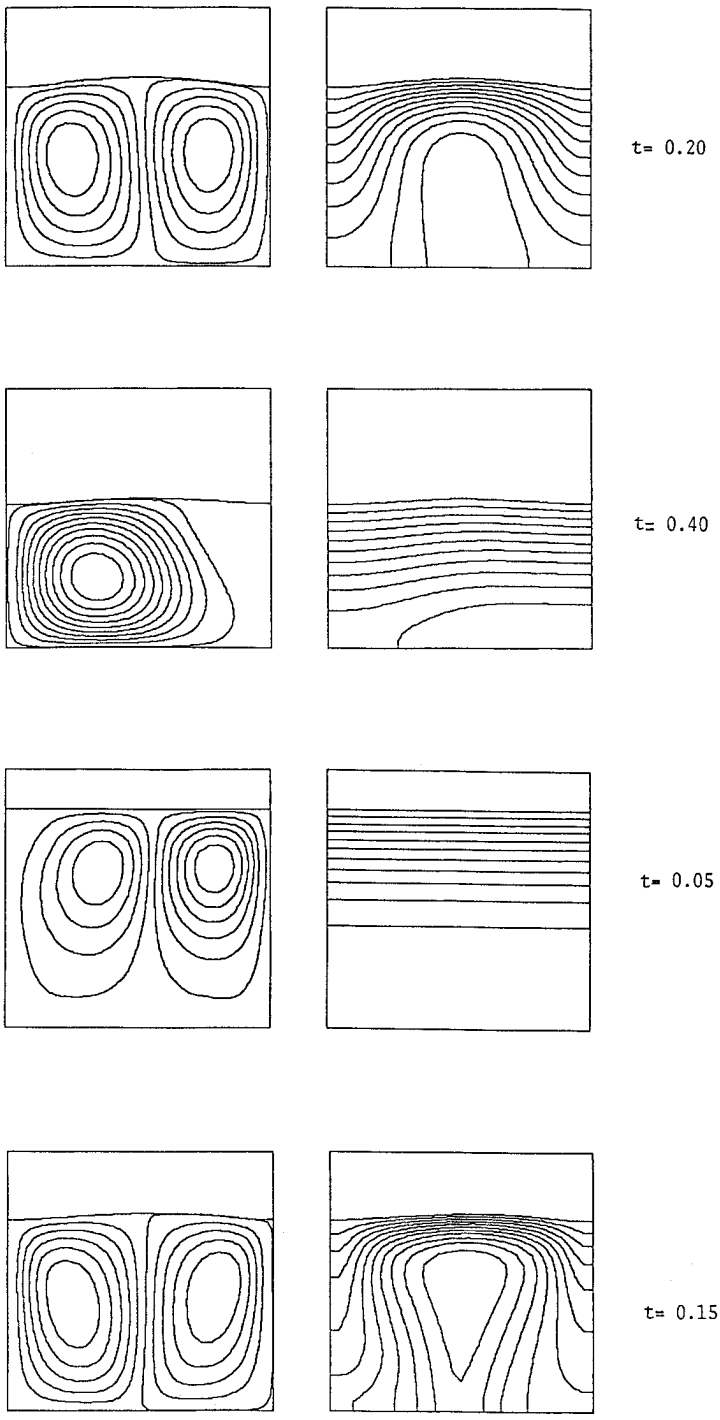

Figure 9.
Streamlines (left) and isotherms (right) at various times during the solidification process for $St^{l} = St_0^{l}$, $Ra = Ra_0$

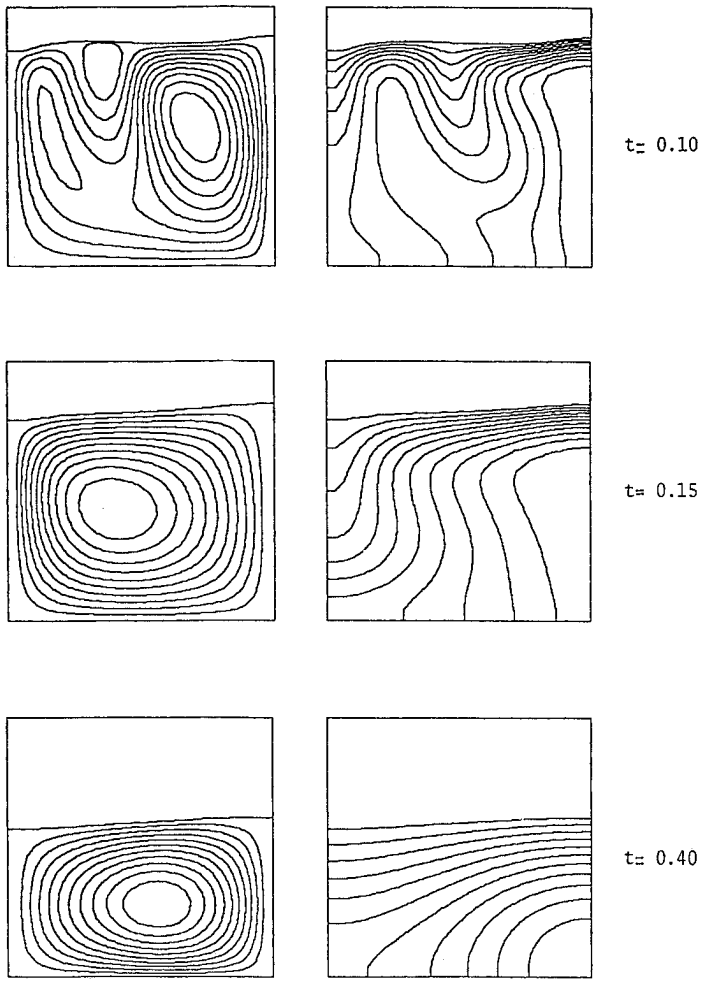

Figure 10a.
Streamlines (left) and isotherms (right) at various times during the solidification process for $St' = 3St'_0$, $Ra = 3Ra_0$

from the isotherm patterns that a thermal boundary layer is formed along the solid-liquid interface shortly after the onset of convection, but disappears at later times, while the fluid in the lower part of the cavity is horizontally stratified due to the effect of the adiabatic bottom wall. By examining the flow field at the later stage of its development, one can note that the convection is still relatively strong while the effective Rayleigh number already falls well below the Bénard critical value (i.e. $4\pi^2$). More remarkably, the flow and temperature fields are not symmetric with respect to the centerline ($x = L/2$) of the cavity. This is in contrast with the results of melting from below where the flow and isotherm patterns are perfectly symmetric with respect to the centerline during the whole melting process, as have been obtained by Zhang *et al.* (1991). The asymmetry of the flow and temperature fields in the present

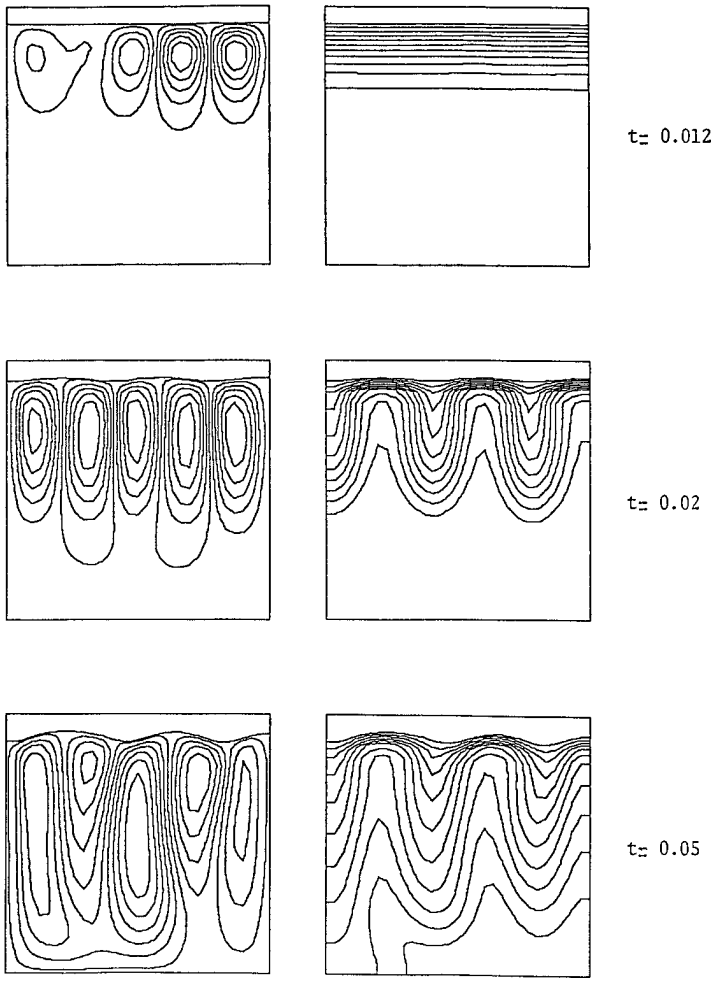

Figure 10b.

case is essentially due to its transient character during the whole cooling process where the initial perturbations at the onset of convection are playing a dominant role. In other words, the results obtained here show the growth and decay of arbitrary (numerical) perturbations while energy is continuously extracted from the flow domain via the solidification process. Under these circumstances, an asymmetric solution thus seems rather "natural" . However, as the governing equations and boundary conditions are symmetric for $x \rightarrow -x$, the solution obtained here is just one of a pair, the other being its mirror image about the centerline $x = L/2$, with an equal probability of occurring. These results clearly show that the development of convection during the solidification process in a cavity cooled from above is completely different from the melting process in a cavity heated from below (Zhang *et al.,* 1991). In

other words, the results obtained in one case cannot be applied or generalized to the other, as it is usually done when convection is neglected and only conduction is taken into account.

On the basis of these results, it can be concluded that the solidification process of a superheated fluid can be divided into three distinct stages:

(1) *The conduction stage*: at this early stage, convection cannot yet develop and the solidification as well as the cooling of the fluid are simply governed by conduction heat transfer. The time scale of this stage is a decreasing function of the superheat.

(2) *The convection stage*: as long as the effective Rayleigh number corresponding to the thermally unstable layer beneath the solid-liquid interface is high enough to maintain the Bénard convection, its effect is essentially to evacuate the superheat from the cavity and to slow down the solidification rate, and even to remelt the solid phase. The time scale in this stage is governed by the convective cooling process.

(3) *The pure conduction stage*: at the end of the convection regime, the superheat is reduced to zero and the fluid is at its freezing point. The solidification process is then governed by conduction in the solid phase only. This stage is completely determined by the well-known Neumann solution of the classic Stefan problem with a time scale of the order of $\sqrt{t}$.

The overall effect of convection on the solidification process is represented in Figure 5, which shows that neglecting the effect of convection amounts to over-estimating the solidification time by about 12 percent if $Ra = 800$ and $St^{l} = 0.67$.

Conclusion

A study has been made of the solidification of a superheated fluid contained in a rectangular porous cavity whose upper boundary is maintained at a temperature below the freezing point, while all other boundaries are perfectly insulated. It was found that the development of convection during the solidification from above is quite different from that observed in the melting from below. While the overall effect of convection is to reduce the total solidification time, it actually slows down the solidification rate during its most active period, where the enhanced heat transfer essentially contributes to evacuate the superheat of the fluid, and even to melt the solid phase.

Finally, it should be noted that while some studies have been made of the solidification of a superheated fluid in a cavity with one boundary maintained at a temperature above the freezing point, while another (opposite) wall is subjected to a subcooling temperature, no study has been made (to our knowledge) of the problem considered here, i.e. the solidification of a cavity with the upper boundary subcooled and all other walls adiabatic. Although in almost all phase change problems, the heat transfer mechanism has been recognized to involve both conduction and convection, the present process is characterized by a succession of three distinct stages as described in the preceding section, namely:

(1) The conduction stage, where both the liquid and solid phases are governed by conduction.

(2) The convection stage, where convection dominates the cooling process of the superheated fluid while conduction controls the heat removal through the solid phase.

(3) The pure conduction stage, where solidification is completely governed by conduction in the solid, with no heat transfer in the remaining liquid.

References

Bejan, A. (1989), "Theory of melting with natural convection in an enclosed porous medium", *J. Heat Transfer,* Vol. 111, pp. 407-15.

Boger, D.V. and Westwater, J.W. (1967), "Effect of buoyancy on the melting and freezing process", *J. Heat Transfer,* Vol. 89, pp. 81-9.

Chellaiah, S. and Viskanta, R. (1988), "Freezing of saturated and superheated liquid in porous media", *Int. J. Heat and Mass Transfer,* Vol. 31 No. 2, pp. 321-30.

Chellaiah, S. and Viskanta, R. (1989), "Freezing of water-saturated porous media in the presence of natural convection: experiments and analysis", *J. Heat Transfer,* Vol. 111, pp. 425-32.

Jany, P. and Bejan, A. (1988), "The scales of melting in the presence of natural convection in a rectangular cavity filled with porous medium", *J. Heat Transfer,* Vol. 110, pp. 526-9.

Prud'homme, M. and Nguyen, T.H. (1989), "Solidification par perturbations singulières pour un problème de Stéfan généralisé", *Int. J. Heat Mass Transfer,* Vol. 32 No. 8, pp. 1501-15.

Prud'homme, M., Nguyen, T.H. and Nguyen, D.L. (1989), "A heat transfer analysis for solidification of slabs, cylinders and spheres", *J. Heat Transfer,* Vol. 111, pp. 669-705.

Zhang, X. and Nguyen, T.H. (1990), "Development of convective flow during the melting of ice in a porous medium heated from above", *ASME HTD,* Vol. 156, pp. 1-6.

Zhang, X., Nguyen, T.H. and Kahawita, R. (1991), "Melting of ice in a porous medium heated from below", *Int. J. Heat and Mass Transfer,* Vol. 34 No. 2, pp. 389-406.